THE JOURNAL OF BIOLOGICAL CHEMISTRY
Vol. 279, No. 37, Issue of September 10, pp. 39132–39138, 2004

Printed in U.S.A.

Crystal Structure of Human Bisphosphoglycerate Mutase*

Received for publication, May 28, 2004, and in revised form, June 28, 2004
Published, JBC Papers in Press, July 16, 2004, DOI 10.1074/jbc.M405982200

Yanli Wang‡§, Zhiyi Wei‡§, Qian Bian§, Zhongjun Cheng‡§, Mao Wan§, Lin Liu‡§, and Weimin Gong‡§¶

From the ‡National Laboratory of Biomacromolecules, Institute of Biophysics, Chinese Academy of Sciences, Beijing 100101, China and the §School of Life Sciences, Key Laboratory of Structural Biology, University of Science and Technology of China, Hefei, Anhui 230026, China

Bisphosphoglycerate mutase is a trifunctional enzyme of which the main function is to synthesize 2,3-bisphosphoglycerate, the allosteric effector of hemoglobin. The gene coding for bisphosphoglycerate mutase from the human cDNA library was cloned and expressed in *Escherichia coli*. The protein crystals were obtained and diffract to 2.5 Å and produced the first crystal structure of bisphosphoglycerate mutase. The model was refined to a crystallographic *R*-factor of 0.200 and R_{free} of 0.266 with excellent stereochemistry. The enzyme remains a dimer in the crystal. The overall structure of the enzyme resembles that of the cofactor-dependent phosphoglycerate mutase except the regions of 13–21, 98–117, 127–151, and the C-terminal tail. The conformational changes in the backbone and the side chains of some residues reveal the structural basis for the different activities between phosphoglycerate mutase and bisphosphoglycerate mutase. The bisphosphoglycerate mutase-specific residue Gly-14 may cause the most important conformational changes, which makes the side chain of Glu-13 orient toward the active site. The positions of Glu-13 and Phe-22 prevent 2,3-bisphosphoglycerate from binding in the way proposed previously. In addition, the side chain of Glu-13 would affect the Glu-89 protonation ability responsible for the low mutase activity. Other structural variations, which could be connected with functional differences, are also discussed.

Bisphosphoglycerate mutase (BPGM)[1] is an erythrocyte-specific trifunctional enzyme. The main activity is that of synthase (BPGM, EC 5.4.2.4), catalyzing the formation of 2,3-bisphosphoglycerate (2,3-BPG) from 1,3-bisphosphoglycerate (1,3-BPG) (1–3) (see Fig. 1*A*). The second activity is that of a mutase (phosphoglycerate mutase, EC 5.4.2.1) catalyzing the interconversion between 2- and 3-phosphoglycerate (Fig. 1*B*) (4). The third activity, as a phosphatase (*S*-succinylglutathione hydrolase, EC 3.1.3.13), is to catalyze the hydrolysis of 2,3-BPG to 3- or 2-phosphoglycerate and a phosphate (Fig. 1*C*) (1, 2). The phosphatase reaction can be stimulated by a number of anions including chloride, phosphate, and particularly by 2-phosphoglycolate (5). These three enzymic activities have been found to occur at a unique active site with two different binding sites for the substrates, one for bisphosphoglycerate and another for monophosphoglycerate (6, 7).

BPGM regulates the level of 2,3-BPG in human blood cells. *In vivo*, the concentration of 2,3-BPG is determined by the relative activities of the synthase and phosphatase reactions. In red blood cells, 2,3-BPG is the main allosteric effector of hemoglobin. It shifts the equilibrium between the oxy and deoxy conformations of hemoglobins by preferentially stabilizing the unliganded form. Sickle cell anemia is characterized by polymerization of deoxygenated hemoglobin mutants giving rise to deformed erythrocytes and vaso-occlusive complications. 2,3-BPG has been shown to facilitate this polymerization. The ability to modulate the 2,3-BPG level *in vivo* would have important implications in the treatment of ischemia and sick cell anemia. One therapeutic approach would be to decrease the intraerythrocytic level of 2,3-BPG by increasing the phosphatase activity of the BPGM.

Based on its enzymatic properties and amino acid sequence homology, BPGM is closely related to the glycolytic housekeeping enzyme, cofactor (2,3-BPG)-dependent phosphoglycerate mutase (dPGM) (8, 9), involved in glycolytic and gluconeogenic pathways with sequence identities in the 40–50% range (6). In the SCOP data base, BPGM and dPGM are grouped into a superfamily along with fructose-2,6-bisphosphatases and acid phosphatase. Sequence and structural comparisons show that they share a set of conserved residues forming the catalytic core but otherwise exhibit many differences associated with substrate specificities and catalytic activities. For example, the synthase activity of BPGM is higher than dPGM, but the latter has stronger mutase activity.

A modest resolution structure of dPGM from *Saccharomyces cerevisiae* was reported in 1974 (10). Recently, the high-resolution structures of dPGMs and the complex with their inhibitors were reported (11–17). According to these structural results, the substrate binding sites and the mutase catalytic mechanisms have been discussed. However, no BPGM three-dimensional structure information is available, although BPGM has been crystallized (18), Here we report the crystal structure of human BPGM (hBPGM) for the first time. Structural comparison of hBPGM and dPGMs show some significant differences between the two groups of enzymes.

* This work is supported by Project 200128 from the Foundation for Authors of National Excellent Doctoral Dissertation of China, Grant 30225015 from the National Foundation of Talent Youth, Grant 2001AA233021 from the National High Technology Research and Development Program of China, Grant 2002BA711A13 from the 863 Special Program of China, the Key Important Project and other projects from the National Natural Science Foundation of China (Grant No. 30121001, No. 30070170, No. 30130080 and No. 30121001), and Grant KSCX1-SW-17 from the Chinese Academy of Sciences. The costs of publication of this article were defrayed in part by the payment of page charges. This article must therefore be hereby marked "*advertisement*" in accordance with 18 U.S.C. Section 1734 solely to indicate this fact.

The atomic coordinates and structure factors (code 1T8P) have been deposited in the Protein Data Bank, Research Collaboratory for Structural Bioinformatics, Rutgers University, New Brunswick, NJ (http://www.rcsb.org/).

¶ To whom correspondence should be addressed: Institute of Biophysics, 15 Datun Rd., Chaoyang District, Beijing 100101, China. Tel.: 86-10-64888467; Fax: 86-551-3607154; E-mail: wgong@sun5.ibp.ac.cn.

[1] The abbreviations used are: BPGM, bisphosphoglycerate mutase; hBPGM, human BPGM; dPGM, cofactor-dependent phosphoglycerate mutase; BPG, bisphosphoglycerate.

EXPERIMENTAL PROCEDURES

Gene Cloning, Expression, and Protein Purification—The hBPGM gene was amplified from human brain cDNA library (Clontech) by a PCR using the 5′- and 3′-end special primers 5′ CATATGTCCAAGTACAAACTTATTATG 3′ and 5′ CTCGAGTTTTTTAGCTTGTTTCAC 3′ (Sangon) designed based on the mRNA sequence of hBPGM (GenBank™ accession number X04327). Those oligonucleotides were introduced with NdeI and XhoI restriction sites, respectively. *Taq* polymerase, T-vector, DNA ligase, and the relevant restriction enzymes were obtained from Takara. The polymerase chain reaction product (~800 bases) was purified with the Gel Extraction mini kit (Watson BioTechnologies) and cloned into a T-vector. The positive clones were identified by restriction digestion. The DNA fragment was ligated into the NdeI/XhoI-cleaved plasmid pET22b (Novagen) to give the pET22b-hBPGM construction that was amplified in *E. coli* BL21 (DE3). The recombinant protein contains eight non-native residues at the C terminus. The integrity of the gene was confirmed by DNA sequencing. Single colonies were cultured in Luria-Bertani broth medium with ampicillin (100 μg ml^{-1}) for expression. Cells were induced with 0.5 mM isopropyl-β-D-thiogalactopyranoside after attaining an A_{600} of 0.4 and grown for an additional 4 h at 310 K. The cells were harvested by centrifugation, resuspended in lysis buffer containing 0.5 M NaCl, 20 mM Tris-HCl (pH 7.5), and lysed by sonication on ice. After centrifugation, the supernatant was loaded onto a nickel-nitrilotriacetic acid column (Qiagen) and eluted using a step gradient of 0.05–0.5 M imidazole. The fractions were tested for purity by SDS-PAGE. The purified human BPGM protein was desalted and concentrated to 30 mg ml^{-1}, determined by a Bio-Rad Protein Assay. Sample purity and molecular weight (~30 kDa) were verified by SDS-PAGE and mass spectrometry, respectively.

Crystallization and Data Collection—Crystals were grown by hanging drop vapor diffuse method at 291 K from a protein solution containing hBPGM (30 mg ml^{-1}), 20 mM Tris-HCl (pH 7.5) with 50 mM NaCl and an equal volume reservoir solution comprising 100 mM HEPES-NaOH (pH 7.0) and 20% (w/v) polyethylene glycol 6000. Crystals appeared after 3 days and kept growing for a week. The diffraction data were collected on a Mar-CCD detector at the Beijing Synchrotron Radiation Facility (λ = 0.9 Å) at the Institute of High Energy Physics, Chinese Academy of Science. A total of 200 frames of data to 2.5 Å were collected with oscillation range of 1° at 100 K. Data were processed with Denzo and Scalepack (19).

Structure Determination and Refinement—Molecular replacement was performed with program AmoRe (20) using data from 15 to 3.5-Å resolution with *S. cerevisiae* dPGM (PDB entry: 5PGM) as the searching model. Multiple cycles of refinement were performed with package of CNS (21). The non-crystallography symmetry was applied during all steps of refinement. Water molecules were included near the end of refinement, followed by manual modification in the graphics program O (22). The quality and stereochemistry of the final model was analyzed with PROCHECK (23).

RESULTS AND DISCUSSION

Structure Determination

Crystals grew with a rod-shaped morphology and belonged to space group $P2_1$ based on the systematic absences in the diffraction data. The unit cell dimensions are a = 38.6 Å, b = 61.8 Å, c = 123.3 Å, β = 95.0° with a solvent content of 48% corresponding to two monomers for each asymmetric unit. The final model refined at a 2.5-Å resolution contains residues from Ser-2 to Asp-250 of the total 267 residues (including the His tag) in each monomer with no definite electron density beyond residue 250. The data in Table I show a well refined structure with excellent stereochemistry. In the Ramachandran plot, 91.4% of the residues are located in the most favored areas, and 8.1% are located in the additional allowed regions. Only one residue, Ser-24, is located at generously allowed regions (discussed below). The model fits well with the corresponding electron density except for the C-terminal residues.

Overall Structure

The hBPGM monomer (Fig. 1)contains two domains including six β-strands (named βA–F) and ten α-helices (named α1–10). The α/β-fold of hBPGM resembles that of the dPGMs from *S. cerevisiae* and *E. coli* (Fig. 2). The protein core consists of a six β-strand in the order βA, βB, βC, βD, and βF in parallel and strand βE in antiparallel conformations. The β-sheet is flanked by six α-helices.

The C-terminal tail ends around the active site. Glu-249 and Asp-250 lie on the center of the active cleft mouth with their side chains oriented from the active cleft. Lys-246 is hydrogen bonded to OE-1 of Glu-249 via its NZ atom. The OE-1 atom of Glu-33 interacts with the NZ atom of Lys-247 by a hydrogen bond. It is noteworthy that there is always an acidic residue at

TABLE I
Summary of data collection and structure refinement

Numbers in parentheses represent the value for the highest resolution shell.

Unit cell (Å °)	a = 38.6 b = 61.8 c = 123.3 β = 95.0
Resolution limit (Å)	30–2.5 (2.61–2.5)
Completeness (%)	96.0 (97.2)
Number of reflections	176,376
Number of independent reflections	18,907
R_{merge}	0.058 (0.183)
I/σ	9.94 (4.14)
R-factor[a]	0.200 (0.302)
R_{free}[b]	0.266 (0.337)
Number of non-H atoms	4,221
Protein atoms	3,989
Water molecules	232
Average B-factors (Å^2)	
Main chain	36.68
Side chain	37.63
Water	39.88
Root mean square distance of bond lengths (Å)	0.007
Root mean square distance of bond angles (°)	1.34

[a] R-factor = $\Sigma||F_{obs}| - |F_{calc}||/\Sigma|F_{obs}|$, where F_{obs} and F_{calc} are observed and calculated structure factors.

[b] R_{free} = ΣSUB$||F_{obs}| - |F_{calc}||/\Sigma T|F_{obs}|$, where T is a test data set of 10% of the total reflections randomly chosen and set aside prior to refinement.

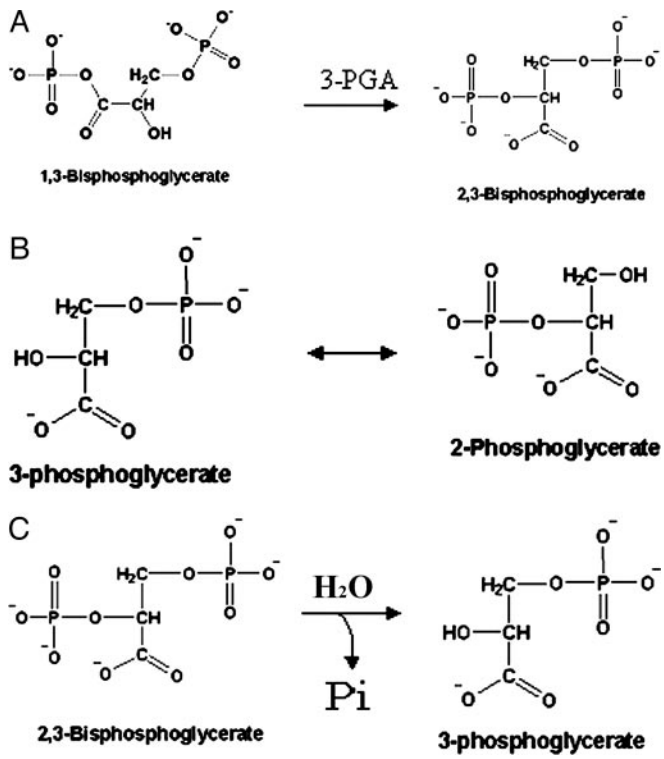

FIG. 1. **Reactions catalyzed by BPGM.** *A*, synthase activity; *B*, mutase activity; *C*, phosphatase activity.

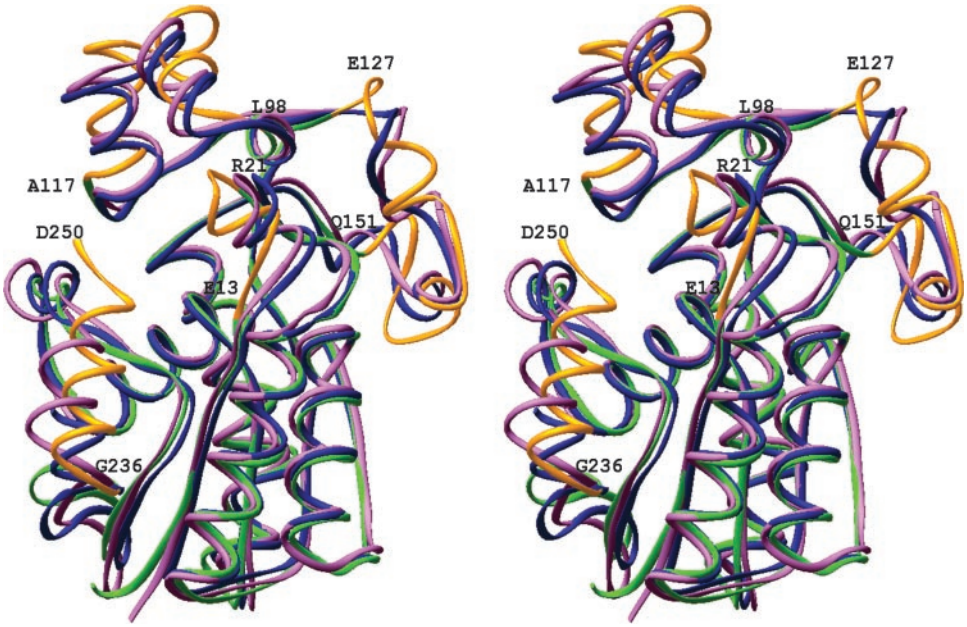

FIG. 2. **Stereo view of the structural superposition of the hBPGM (*green*), *E. coli* dPGM (*purple*), and *S. cerevisiae* dPGM (*blue*).** The regions (residue 13–21, 98–117, 127–151, and the C-terminal tail of hBPGM) whose conformations are different from PGM are colored in *yellow*. This figure was produced using the Lsqman (24) and Ribbons (25) programs.

residue 33 in BPGMs. These interactions may make the C-terminal helix (helix 10) more stable and fix it to the active site pocket. The values of the *B*-factors indicate that the C-terminal region is more flexible compared with the other parts of the molecule. Similarly, in the C-terminal tail, 12 residues cannot be observed in *S. cerevisiae* dPGM and 9 residues are missing in *E. coli* dPGM in its unphosphorylated form. The C-terminal residues play an important role in the activities of the enzymes in this family. Removal of the 12 C-terminal residues from *S. cerevisiae* dPGM is associated with loss of mutase activity but no change in phosphatase activity (26). The deletion of the last seven residues completely abolished the three catalytic activities of the hBPGM (9). The C-terminal residues would be involved in transferring a phosphoryl group to the internal active site (27). Therefore, the disordering of the C-terminal tail appears to be a common feature in both of BPGMs and of dPGMs and could accommodate the access of the substrate to the active site.

FIG. 3. **The dimer of hBPGM viewed along the non-crystallographic 2-fold axis.**

Dimer Association

hBPGM forms a dimer in the crystal in agreement with those observed in solution (5). The dimer is formed between the surface of the βC strands and α3 helices of the two monomers with a non-crystallographic 2-fold symmetry (Fig. 3) similar to *E. coli* dPGM and *S. cerevisiae* dPGM. The side chains of Ile-64, Trp-68, Leu-69, Leu-71, and Val-81 form a hydrophobic dimerization core. Specifically, the side chains of Trp-68 from both monomers stack with each other across the 2-fold axis. Those hydrophobic residues are conserved in all BPGMs and the dimerized dPGMs but not in *Schizosaccharomyces pombe* dPGM, which is a monomer. In addition, the salt bridge between Lys-29 and Glu-72 and several hydrogen bonds formed by Glu-51, Phe-52, Asp-53, His-65, Glu-77, and Arg-140 strengthen the dimer interactions. Arg-140 forms two hydrogen bonds to the carbonyl oxygen of Phe-52 and to the OD-2 atom of Asp-53 via its NH_2 atom and forms a hydrogen bond to the OE-1 atom of Glu-51 via its NE atom. His-65 forms a hydrogen bond to the side chain of Glu-77 via its NE-2 atom. All of these residues discussed above are conserved in BPGMs. The two subunits of the dimer show few differences when overlaid. The root mean square distance between their Cα atoms is 0.51 Å. The following discussion is based on the structure of monomer A.

Comparison with dPGMs

Sequences Alignment and Backbone Comparison—Similarities of the hBPGM structure to some dPGM structures (PDB codes 5PGM, 1E58, 1E59, 1QHF, and 1FTZ) were analyzed using the program DALI (28) and LSQMAN (24). A structure-based sequence alignment of BPGMs and dPGMs is shown in Fig. 4. The sequence of hBPGM is ~50% identical to dPGMs. The catalytic site residues Arg-10, His-11, Arg-62, Glu-89, Arg-90, Arg-116, Arg-117, and His-188 are conserved in all of them. However, some residues involved in the substrate binding in dPGMs have been substituted in BPGMs (discussed below).

The topology of the α/β domain of BPGM shows considerable similarity to dPGMs. A superposition of hBPGM with the structure of *S. cerevisiae* dPGM and *E. coli* dPGM yields root mean square distances of 0.69 and 0.74 Å, respectively, for Cα atoms in 124 residues in three regions (hBPGM residues 4–11, 25–97, and 157–199), indicating strong structural homology within

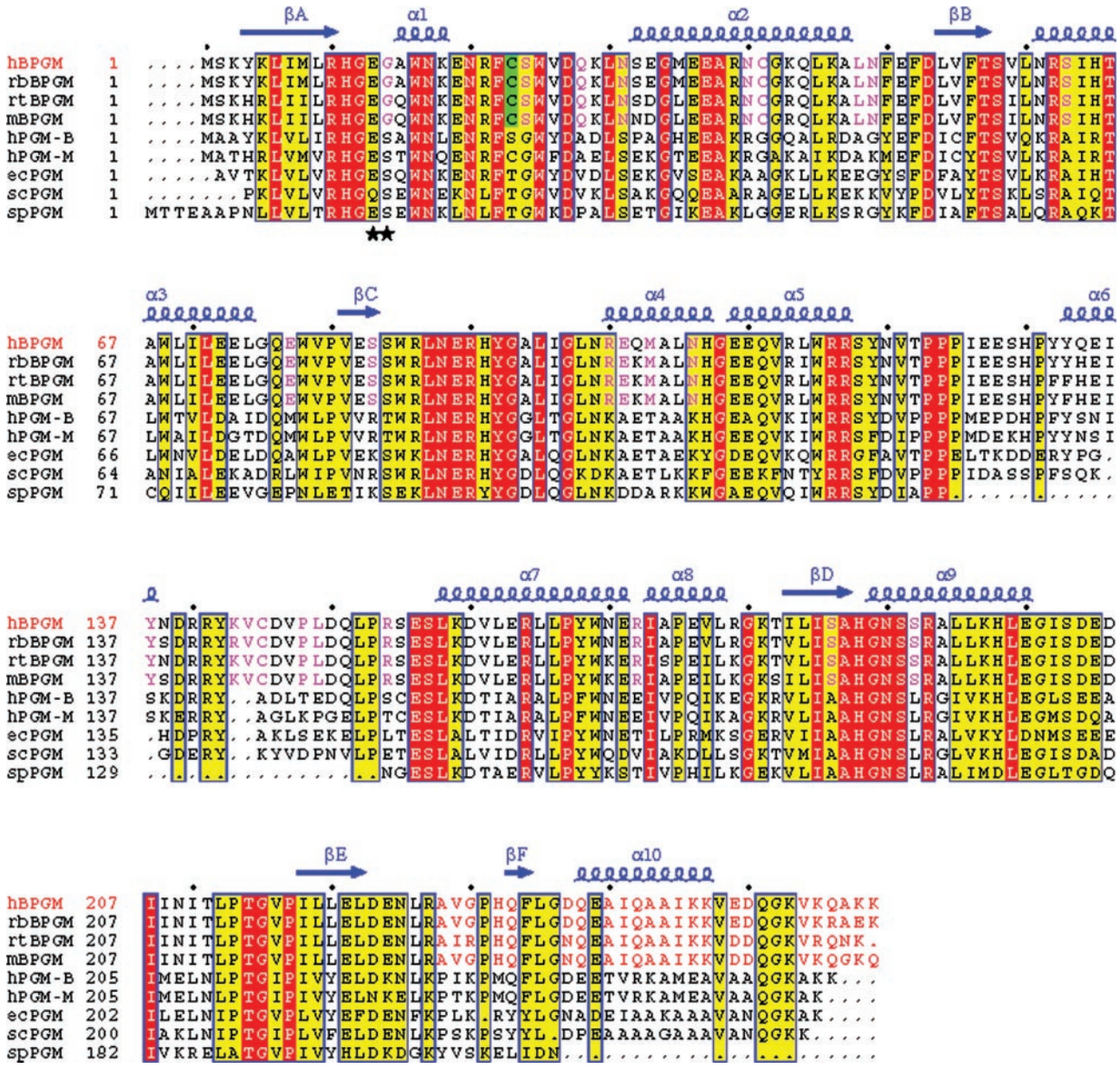

FIG. 4. **Structure-based sequence alignment of BPGMs from human (*hBPGM*), rabbit (*rbBPGM*), rat (*rtBPGM*), and mouse (*mBPGM*) and dPGMs from human brain (*hPGM-B*), human muscle (*hPGM-M*), *E. coli* (*ecPGM*), *S. cerevisiae* (*scPGM*), and *S. Pombe* (*spPGM*).** The secondary structure elements in the crystal structure of hBPGM are shown above the alignment in *blue*. *Arrows* indicate β-strands and *coils* indicate helices. Strictly conserved and conservatively substituted residues are *boxed* and marked with *red* and *yellow background*, respectively. Residues conserved only for BPGMs are colored in *purple*. The residues in the C-terminal region that are different between BPGMs and dPGMs are colored in *red*. Cys-23 is present in all BPGMs and human muscle dPGM, resulting in their sensitivity to Hg^{2+}, and marked in *green background*. Glu-13 and Gly-14 are marked by *black stars*. Every 10 residues of the hBPGM sequence are marked with *dots* and the residue numbers in each sequence are showed in the front. The figure was generated using ESPript (29).

those regions, consistent with the concept that BPGM and dPGM are structurally homologous enzymes. The most significant variations in the backbone occur in the regions 13–21, 98–117, 127–151, and the C-terminal tail (Fig. 2). With a four-residue insertion at residues 136, 137, 143, and 144, an additional α-helix is formed from residue 133 to 138, resulting in the different conformations at the region of residues 127–151. This region is far away from the active site, and the structural differences would not contribute to the catalytic activity. The fragments 13–21, 98–117, and the C-terminal fragment surround the active site. These conformational changes may have significant effect on the enzymatic activity.

Residues Specific for BPGMs—There are 24 residues (Fig. 4, *pink*) that are identical in BPGMs but differ from those in dPGMs. Among them, Glu-77 is involved in the interactions between the two subunits by forming a hydrogen bond with His-65. Ser-63 and Ser-186, in which the equivalent residues are both Ala in dPGMs located near the active site, form two hydrogen bonds between their main-chain and side-chain oxygen atoms. The hydroxyl oxygen of Ser-192 forms three hydrogen bonds with the carbonyl oxygen atoms of His-188 and Gly-189, and the main-chain nitrogen atom of Arg-193. These additional hydrogen bonds may help stabilize the structure.

Gly-14 is a critical BPGM-specific residue. A mutation of Gly-14 of hBPGM to Ser did not modify the synthase activity, whereas the mutase and phosphatase activities were 2-fold increased or decreased, respectively. However, replacing Gly-14 with Arg enhanced phosphatase activity by 28.6-fold, whereas synthase and mutase activities were decreased 10-fold (30). In dPGMs, the equivalent residue Ser interacts with the

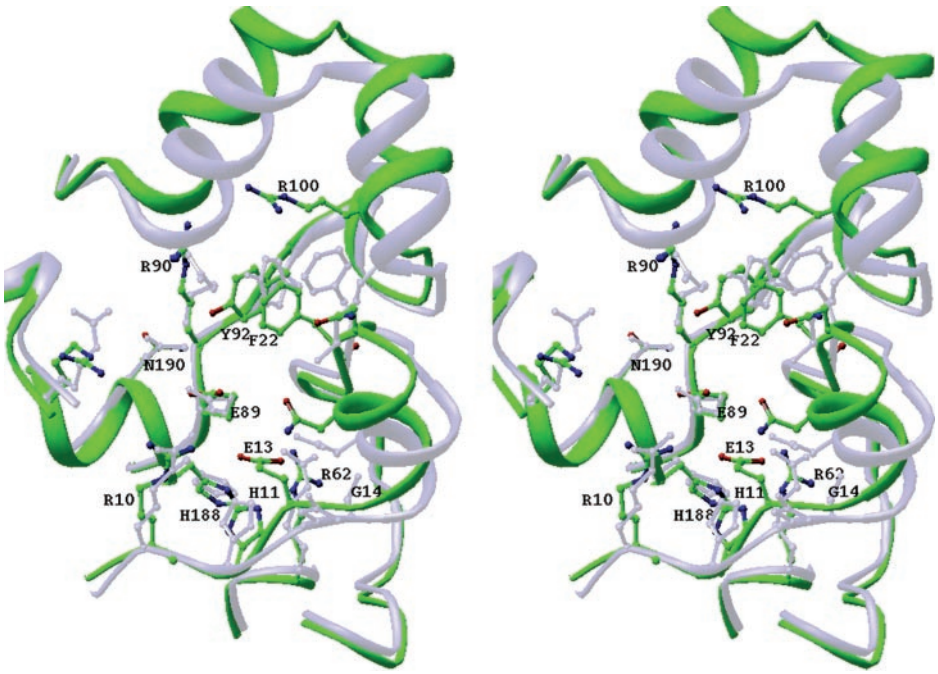

FIG. 5. **Stereo drawing of the superposition of the active site pocket of hBPGM (*green*) and *S. cerevisiae* dPGM (*gray*).** The critical residues in the active site pocket are labeled.

substrate (12). In prostatic acid phosphatase, Arg-15, the equivalent residue of Gly-14 of BPGM, points toward the active site and is involved in the substrate binding too (31–33). Fig. 5 shows that the conformation around Gly-14 varies significantly. As a consequence, the side chain of Glu-13 in hBPGM points toward the active site, forming a hydrogen bond network with Arg-10, His-11, Glu-89, and Gly-189 via three water molecules, whereas the equivalent residue of dPGMs orients away from the active site. Glu-89 is conserved in all BPGMs and dPGMs. In mutase activity, Glu-89 acts as an acid or a base during enzyme phosphorylation and dephosphorylation (12). The phosphotransfer step of the mutase reaction requires a proton to be transferred to or from Glu-89. The hydrogen bond between Glu-13 and the side chain of Glu-89 would affect the protonation ability of Glu-89, so that the mutase activity is lower in BPGMs. In contrast, the first phosphotransfer of the synthase reaction involves the transfer of an acyl-phospho group and does not require a proton to be transferred (6).

Ser-24 is reported to be involved in the binding of both monophosphoglycerates and 2-phosphoglycolate (7). This position is conserved as a Gly in all dPGMs. It was proposed that its backbone nitrogen atom interacts with the substrate carboxylate group (15). Because its dihedral angle is located in a general allowed region in the Ramachandran plot, it was predicted that Ser-24 would be the major reason for the different enzymatic activities of BPGMs and dPGMs by adopting a different dihedral values and changing the main-chain conformation (12, 15). In our hBPGM structure, no significant structural change was observed except the side chain of Ser-24 was added. Although the Ser-24 side chain fits the electron density well, its conformation is in an unfavorable region of the Ramachandran plot (Fig. 6). The unfavorable stereochemistry may be compensated by the formation of a hydrogen bond between its hydroxyl oxygen and the backbone nitrogen atom of Tyr-92. Its carbonyl oxygen maintains contact with the NH_2 atom of Arg-62 as in dPGMs. So it is unlikely that Ser-24 plays an important role in distinguishing the activities of BPGMs and dPGMs.

Active Site and the Substrate Binding Pocket—The active site pocket was found at the carboxyl end of the parallel β-strands of the α/β-domain. His-11 and His-188 are located at the bottom of the active site pocket as well as Arg-10 and Arg-62. The mouth of the cleft is defined by Lys-18, Asn-20, Arg-100, and Arg-116 on one side and Ile-208, Asn-209, and Thr-211 on the other side (Fig. 5). Residues 246–250 lie on the surface of the active site pocket. The general shape of the active cleft looks similar to those of dPGMs, but the details differ resulting from the conformational changes at regions of 13–21, 98–117, and the C termini. The catalytic site cleft contains many basic residues resulting in a highly positive electrostatic potential accommodating for the negative charged substrates as dPGMs.

His-11 and His-188 are conserved in BPGMs and dPGMs. In the hBPGM structure, their side chains adopt very similar conformations to those in the structure of dPGM (Fig. 5). His-11 was proposed to accept a phosphate group during the reactions (6). His-188 was confirmed to be very important for catalysis, but its precise function is still speculative (34, 35). In the hBPGM structure, the NE-2 atom of His-11 forms a hydrogen bond to the ND-1 atom of His-188. The hydroxyl group of Ser-58 is hydrogen-bonded to atom NE-2 of His-188. This interaction is also conserved in dPGMs in the rat prostatic acid phosphatase (between Thr-75 and His-257) and in fructose-2,6-bisphosphatase (between Ser-52 and His-141), suggesting they contribute to the correct orientation of the His-188 imidazole ring.

Most of the residues involved in bisphosphoglycerate binding (Arg-10, Asn-17, Arg-62, Glu-89, Arg-90, Tyr-92, Arg-116, Arg-117, and Asn-190) are conserved in BPGMs as in dPGMs. Upon a superposition of the structures of hBPGM and dPGMs, Arg-10, Arg-62, Glu-89, Arg-90, and Asn-190 fit well; Asn-17, Arg-116, and Arg-117 shift with the backbone movement. The side chains of Arg-116 and Arg-117 are flexible and cannot be observed in the electron density map.

Thr-20 and Lys-97 (numbered as in dPGMs), in which the side chains were proposed to be involved in 2,3-BPG binding in dPGMs, are substituted by Cys-23, and Arg-100, respectively, in hBPGM. Cys-23 is conserved in BPGMs and in muscle dPGM leading to a susceptibility to inactivation by Hg^{2+} (6). In hBPGM, the guanidinium group of Arg-62, which is necessary for substrate binding, contacts the SH group of Cys-23 in van der Waals distance. If a positively charged Hg^{2+} bound to Cys-23, it should push away the same positively charged

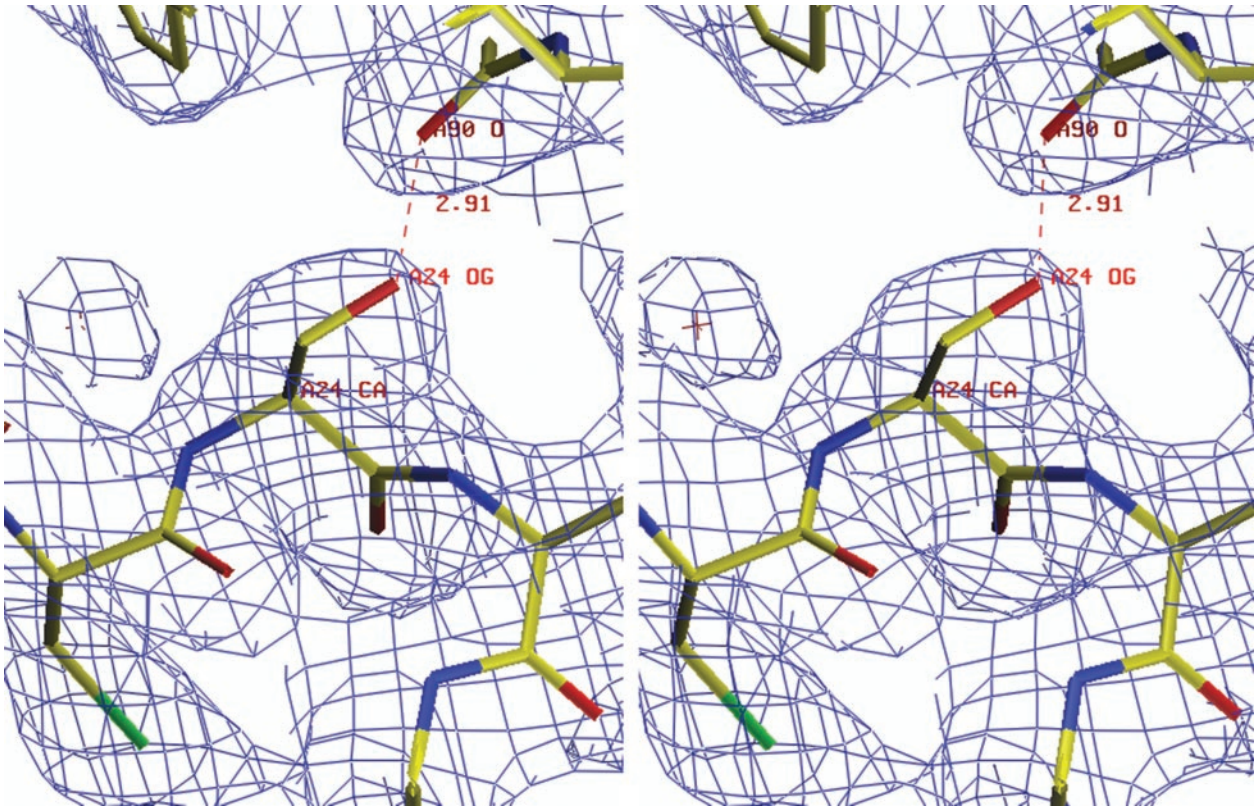

FIG. 6. **The electron density map ($2F_o - F_c$, 1.0 σ) of Ser-24.** The hydrogen bond between Ser-24 and Arg-90 is labeled. The ϕ and ψ angles of this residue are 53.5° and −125.1°, respectively. These two angles in the equivalent residue Gly in *E. coli* dPGM are 61.4° and −130.8°, and in *S. cerevisiae* dPGM are 67.6° and −124.9°, respectively.

Arg-62 and prevent the substrate from binding. It also should be noted that in dPGMs, the side chain of Lys-97 points toward the active site pocket. However, in hBPGM, the equivalent residue Arg-100 turns its side chain away from the active site ~90°, toward the surface of the active cleft. It was reported that the substrate binding is not the rate-limited step, and the different catalytic ability of BPGMs and dPGMs is caused mainly by the phosphorylation rates of 1,3-BPG and 2,3-BPG (36). Whether the moving away of Arg-100 is necessary for the specificity of phosphorylation needs to be investigated further.

Compared with dPGMs, the space around the catalytic His-11 is more crowded in hBPGM. Several backbone and residue differences contribute to this. First, the backbone of residues 13–21 shifts with a distance of 5.0 Å between Glu-19 and its equivalent residue in *S. cerevisiae* dPGM. Second, the side chain of Glu-13 points toward the active site, and the side chain of Phe-22 rotates closer to the catalytic His-11 leading to the small active site space. As the consequence, the 2,3-BPG binding model of *E. coli* dPGM (15) cannot be adopted in hBPGM without the backbone or side-chain movements, because the side chain of Glu-13 leads to the steric clash with the phospho group near the catalytic site, and the side chains of Tyr-92 and Phe-22 lead to steric clash with the distal phospho group of 2,3-BPG. Moreover, the binding model of 3-phosphoglycerate to *S. cerevisiae* dPGM observed experimentally (37) cannot be adopted by hBPGM, in which Glu-13 occupies the position of the ligand, either. If the similar binding mode remains in hBPGM, large conformational changes should happen upon the substrate binding. It also should be noted that the binding of dPGMs with 2,3-BPG is only a theoretical model derived from the complex of *E. coli* dPGM and a liner tetravanadate (15). We are trying to obtain the hBPGM-substrate complex crystals, which will provide deeper insight into the binding and catalytic mechanism.

The narrower active cleft and varieties of residues involved in substrate binding could be another reason for different phosphorylation rates of BPGMs and dPGMs by 2,3- and 1,3-BPG, respectively, which leads to the different mutase and synthase activities. The mutase reaction requires that the 2,3-BPG stay as an intermediate and change its orientation in the active site during each round of catalysis (6). However, in hBPGM, the narrower active site pocket would limit the reorientation of 2,3-BPG. Although in the synthase reaction, 2,3-BPG should be released as a product.

In conclusion, hBPGM is similar in the folding, dimerization pattern, and the active site architectures to dPGMs as predicted from the sequence homology. The major structural variations occur at residues 13–21, 98–117, 127–151, and the C-terminal tail. Gly-14 may have caused the most important conformational changes where the inside flipping of Glu-13, together with the relocation of Phe-22, resulted in a more crowded substrate binding pocket and could prevent 2,3-BPG from binding in the way that was proposed in dPGMs. In addition, the side chain of Glu-13 would affect Glu-89 protonation ability that is critical for the mutase activity.

Acknowledgments—We thank Prof. Peng Liu and Yuhui Dong for synchrotron data collection.

REFERENCES

1. Rose, Z. B. (1968) *J. Biol. Chem.* **243,** 4810–4820
2. Rose, Z. B. (1970) *J. Biol. Chem.* **248,** 1513–1519
3. Rose, Z. B. (1980) *Adv. Enzymol. Relat. Areas Mol. Biol.* **51,** 211–253
4. Rosa, R., Gaillardon, J., and Rosa, J. (1973) *Biochem. Biophys. Res. Commun.* **51,** 36–542
5. Rose, Z. B., and Liebowitz, J. (1970) *J. Biol. Chem.* **245,** 3232–3241
6. Fothergill-Gilmore, L. A., and Watson, H. C. (1989) *Adv. Enzymol. Relat. Areas Mol. Biol.* **62,** 227–313
7. Ravel, P., Craescu, C. T., Arous, N., Rosa, J., and Carel, M. C. (1997) *J. Biol. Chem.* **272,** 14045–14050
8. Hass, L. F., Kappel, W. K., Miller, K. B., and Engle, R. L. (1978) *J. Biol. Chem.* **253,** 77–81

9. Garel, M.-C., Joulin, V., Le Boulch, P., Calvin, M.-C., Prehu, M.-O., Arous, N., Longin, R., Rosa, R., Rosa, J., and Cohen-Solal, M. (1989) *J. Biol. Chem.* **264,** 18966–18972
10. Campbell, J. W., Watson, H. C., and Hodgson, G. I. (1974) *Nature* **250,** 301–303
11. Rigden, D. J., Alexeev, D., Phillips, S. E. V., and Fothergill-Gilmore, L. A. (1998) *J. Mol. Biol.* **276,** 449–459
12. Rigden, D. J., Walter, R. A., Phillips, S. E. V., and Fothergill-Gilmore, L. A. (1999) *J. Mol. Biol.* **286,** 1507–1517
13. Bond, C. S., White, M. F., and Hunter, W. N. (2001), *J. Biol. Chem.* **276,** 3247–3253
14. Rigden, D. J., Bagyan, I., Lamani, E., Setlow, P., and Jedrzejas, M. J. (2001) *Protein Sci.* **10,** 1835–1846
15. Bond, C., White M. F., and Hunter, W. N. (2002) *J. Mol. Biol.* **316,** 1071–1081
16. Rigden, D. J., Mello, L. V., Setlow, P., and Jedrzejas, M. J. (2002) *J. Mol. Biol.* **315,** 1129–1143
17. Uhrinova, S., Uhrin, D., Nairn, J., Price, N. C., Fothergill-Gilmore, L. A., and Barlow, P. N. (2001) *J. Mol. Biol.* **306,** 275–290
18. Cherfils, J., Rosa, R., Garel, M. C., Calvin, M. C., Rosa, J., and Janin, J. (1991) *J. Mol. Biol.* **218,** 269–270
19. Otwinowski, Z., and Minor, W. (1997) *Methods Enzymol.* **276,** 307–326
20. Collaborative Computational Project 4 (1994) *Acta Crystallogr. Sect. D Biol. Crystallogr.* **50,** 760–763
21. Brunger, A. T., Adams, P. D., Clore, G. M., DeLano, W. L., Gros, P., Grosse-Kunstleve, R. W., Jiang, J.-S., Kuszewski, J., Nilges, M., Pannu, N. S., Read, R. J., Rice, L. M., Simonson, T., and Warren, G. L. (1998) *Acta Crystallogr. Sect. D Biol. Crystallogr.* **54,** 905–921
22. Jones, T. A., Zou, J. Y., Cowan, S. W., and Kjeldgaard, M. (1991) *Acta Crystallogr. Sect. A* **47,** 110–119
23. Laskowsky, R. A., MacArthur, M. W., Moss, D. S., and Thornton, J. M. (1993) *J. Appl. Crystallogr.* **26,** 283–291
24. Kleywegt, G. J. (1999) *Acta Crystallogr. Sect. D Biol. Crystallogr.* **55,** 1878–1884
25. Carson, M. (1987) *J. Mol. Graphics* **5,** 103–106
26. Walter, R. A., Nairn, J., Duncan, D., Price, N. C., Kelly, S. M., Rigden, D. J., and Fothergill-Gilmore, L. A. (1999) *Biochem. J.* **337,** 89–95
27. Winn, S. I., Watson, H. C., Harkins, R. N., and Fothergill, L. A. (1981) *Philos. Trans. R. Soc. Lond. B. Biol. Sci.* **293,** 121–130
28. Homl, L., and Sander, C. (1993) *J. Mol. Biol.* **233,** 123–138
29. Gouet, P., Courcelle, E., Stuart, D. I., and Metoz, F. (1999) *Bioinformatics* **15,** 305–308
30. Garel, M. C., Arous, N., Calvin, M. C., Craescu, C. T., Rosa, J., and Rosa, R. (1994) *Proc. Natl. Acad. Sci. U. S. A.* **91,** 3593–3597
31. Schneider, G., Lindqvist, Y., and Vihko, P. (1993) *EMBO J.* **12,** 2609–2615
32. LaCount, M. W., Handy, G., and Lebioda, L. (1998) *J. Biol. Chem.* **273,** 30406–30409
33. Ortlund, E., LaCount, M. W., and Lebioda, L. (2003) *Biochem.* **42,** 383–389
34. White, M. F., and Fothergill-Gilmore, L. A. (1992) *Eur. J. Biochem.* **207,** 709–714
35. White M. F., Fothergill-Gilmore, L. A., Kelly, S. M., and Price, N. C. (1993) *Biochem. J.* **291,** 479–483
36. Rose, Z. B., and Dube, B. (1976) *J. Biol. Chem.* **251,** 4817–4822
37. Glina, S. C., Andrew, R. D., Michail, N. I., John, W. C., and Jenifer, A. L. (1999) *Acta Crystallogr. Sect. D Biol. Crystallogr.* **55,** 1822–1826